# NUMERICAL PREDICTIONS OF WIND TURBINE POWER AND AERODYNAMIC LOADS FOR THE NREL PHASE II COMBINED EXPERIMENT ROTOR

**Earl P.N. Duque[†]**
US Army Aeroflightdynamics Directorate, Aviation RDEC, AMCOM
Army/NASA Rotorcraft Division
Ames Research Center
Moffett Field, CA

**Wayne Johnson[‡]**
Rotorcraft Aeromechanics Branch
Army/NASA Rotorcraft Division
Ames Research Center
Moffett Field, CA

**C.P. vanDam[‡], Regina Cortes[!] and Karen Yee[!]**
Department of Mechanical and Aeronautical Engineering
University of California, Davis
Davis, CA

## ABSTRACT

A blade element momentum (BEM), vortex lattice (VL) and a Reynolds-averaged thin-layer Navier-Stokes method (RaNS) were evaluated for their ability to predict the aerodynamic performance of the Combined Experiment Phase II Horizontal Axis Wind Turbine. To evaluate blade stall modeling, the BEM and VL methods utilized the Du-Selig stall delay model along with experimental and computationally derived airfoil characteristics. To validate the methods, experimental data from the IEA Annex XIV database were used. Additional data reduction was applied to sort the experimental data into steady wind speed bins with known error and to make it suitable for validation of numerical methods. All three methods produce good power and sectional normal force predictions at pre-stall wind conditions. The RaNS method fails to capture the correct aerodynamic performance once the blade begins to stall. The VL and BEM methods show better capability in predicting post stall behavior, however to obtain more accurate power and load predictions they need improved stall delay models and adequate airfoil properties. Predicting the correct inboard stall delay is still a challenge to these methods.

## INTRODUCTION

Accurate, reliable and robust numerical predictions of wind turbine rotor power remain a challenge to the wind energy industry. The literature reports various methods that compare numerical predictions to experiments. The methods vary from Blade Element Momentum Theory (BEM) ( Refs. 1,2 ), Vortex Lattice (VL) (Refs. 3), to variants of Reynolds-averaged Navier-Stokes (RaNS) (Refs. 4,5) The BEM and VL methods consistently show discrepancies in predicting rotor power at higher wind speeds mainly due to inadequacies with inboard stall and stall delay models. The RaNS methodologies show promise in predicting blade stall. However, inaccurate rotor vortex wake convection, boundary layer turbulence modeling and grid resolution have limited their accuracy. In addition, the inherently unsteady stalled flow conditions become computationally expensive for even well equipped research labs.

---

[†] Research Scientist, Senior Member AIAA, Member ASME
[‡] Research Scientist, Member AIAA
[‡] Professor, Member AIAA
[!] Undergraduate Research Assistant

| | | Form Approved |
|---|---|---|
| **Report Documentation Page** | | OMB No. 0704-0188 |

Public reporting burden for the collection of information is estimated to average 1 hour per response, including the time for reviewing instructions, searching existing data sources, gathering and maintaining the data needed, and completing and reviewing the collection of information. Send comments regarding this burden estimate or any other aspect of this collection of information, including suggestions for reducing this burden, to Washington Headquarters Services, Directorate for Information Operations and Reports, 1215 Jefferson Davis Highway, Suite 1204, Arlington VA 22202-4302. Respondents should be aware that notwithstanding any other provision of law, no person shall be subject to a penalty for failing to comply with a collection of information if it does not display a currently valid OMB control number.

| 1. REPORT DATE **JAN 2000** | 2. REPORT TYPE | 3. DATES COVERED **00-00-2000 to 00-00-2000** |
|---|---|---|

| 4. TITLE AND SUBTITLE | 5a. CONTRACT NUMBER |
|---|---|
| **Numerical Predictions of Wind Turbine Power and Aerodynamic Loads for the NREL Phase II Combined Experiment Rotor** | 5b. GRANT NUMBER |
| | 5c. PROGRAM ELEMENT NUMBER |
| 6. AUTHOR(S) | 5d. PROJECT NUMBER |
| | 5e. TASK NUMBER |
| | 5f. WORK UNIT NUMBER |

| 7. PERFORMING ORGANIZATION NAME(S) AND ADDRESS(ES) **US Army Aviation and Missile Command,Army/NASA Rotorcraft Division,Army Aeroflightdynamics Directorate (AMRDEC),Moffett Field,CA,94035** | 8. PERFORMING ORGANIZATION REPORT NUMBER |
|---|---|

| 9. SPONSORING/MONITORING AGENCY NAME(S) AND ADDRESS(ES) | 10. SPONSOR/MONITOR'S ACRONYM(S) |
|---|---|
| | 11. SPONSOR/MONITOR'S REPORT NUMBER(S) |

| 12. DISTRIBUTION/AVAILABILITY STATEMENT **Approved for public release; distribution unlimited** |
|---|

| 13. SUPPLEMENTARY NOTES |
|---|

| 14. ABSTRACT **see report** |
|---|

| 15. SUBJECT TERMS |
|---|

| 16. SECURITY CLASSIFICATION OF: | | | 17. LIMITATION OF ABSTRACT | 18. NUMBER OF PAGES | 19a. NAME OF RESPONSIBLE PERSON |
|---|---|---|---|---|---|
| a. REPORT **unclassified** | b. ABSTRACT **unclassified** | c. THIS PAGE **unclassified** | **Same as Report (SAR)** | **9** | |

**Standard Form 298 (Rev. 8-98)**
Prescribed by ANSI Std Z39-18

Although numerical power predictions have been compared to experiment, good wind turbine data of sufficient quality for code validation remains scarce. The data usually come from measurements taken on field installed wind turbines. The joint effort undertaken by several European Union research labs and the United State's National Renewable Energy Laboratory (NREL) has documented and made available experimental field data for several different wind turbines (Refs. 6). Users and numerical analysts have ready access to this data, known as IEA Annex XIV, by either extracting it from the written report or by downloading the electronic data files from an FTP server.

However, users will find that the IEA Annex XIV data contain considerable unsteadiness in the measured power and loads. This variation exists even though the data has been reduced and sorted into specific wind speed and yaw categories. Numerical analysts would find it difficult to validate their computations against this data without further and considerable data reduction.

This paper brings together a comparison of power predictions as obtained by the three different methods - BEM, VL, and RaNS. The predictions use ,as a benchmark, experimental data that has been gleaned from the IEA Annex XIV download site for the NREL Combined Experiment phase II rotor. These comparisons will show data that has been further reduced into steady wind and zero yaw conditions suitable for comparisons to "steady wind" rotor power predictions. The paper presents and discusses the capabilities and limitations of the three numerical methods. In addition, it makes available a reduced set of experimental data suitable for others to validate their work.

## METHODOLOGY

### Experimental Data

The experimental data used in the comparisons was obtained from the NREL Combined Experiment. Phase II Experiment (Refs. 7, 8). This turbine is a highly instrumented downwind, three-bladed, HAWT with rectangular blade planform. Over the years, NREL has taken extensive surface pressure, flow visualization, meteorological and loads data from this field installed turbine.

The Phase II configuration has a rotor that rotates at a constant 72 rpm and rated at 20 kW of electrical power. This fixed-pitch rotor has a diameter of 10.1 meters, untwisted blades, and constant chord of 0.458 meters. The rotor uses the NREL S809 airfoil through out the span with some modifications towards the root to blend with the hub spar. The rotor hub is fixed at a pre-cone of $3^o$ and a fixed pitch

of $12^o$. The rotor hub is mounted onto a nacelle that contains the transmission and electrical power generation equipment. This assembly sits atop a 0.405-meter diameter cylindrical tower 16.8 meters above the ground.

The three blades have flush mounted pressure taps and total pressure probes at several radial locations. In addition to the pressure data, NREL recorded the rotor torque and bending loads as well as angle of attack at several radial stations. The inflow conditions for the turbine were measured by a vertical plane array of sensors positioned nominally upstream of the rotor. The details of NREL's Combined Experiment are covered in Refs. 7 and 8.

To properly validate any predictive method, one needs quality experimental data with documented uncertainty. This requirement for error analysis in the data presentation becomes even more important in wind turbine predictions because of the large fluctuations in the wind, the nacelle yaw errors, and inherent unsteady blade aerodynamics.

For the non-yawed rotor conditions, the IEA Annex XIV provides five sixty-second long averaged wind speed bins. Over this sixty-second sample, there may be large wind speed variations and yaw error. Therefore, we set out to extract "steady" conditions from the IEA database. To accomplish this task, each of the five original averaged wind speed bins was sampled to identify sets of five consecutive rotor revolutions whose standard deviation was less than 0.5 m/s . These sets of five were then further reduced to eliminate those with excessive variance between the minimum and maximum wind speeds and yaw error.
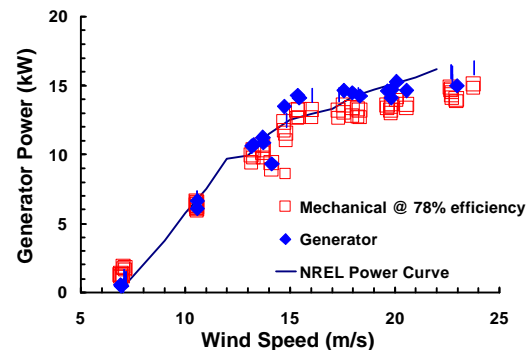


**Figure 1: Experimental power curves referenced to generator**

This process produced seven sets of data each containing five rotor revolutions with average wind speeds of 7.0, 10.5, 13.6, 15.3, 17.8, 20.0 and 23.0 m/s. The data show considerable variations in power at the various wind speed bins. Figure 1 illustrates the cycle averaged generator and mechanical power for each of the 5 revolutions as compared to the NREL power curve published in the Annex XIV report. The generator power and the published NREL power curve show good

agreement in the lower power levels. However there are some differences in the stall regions (wind speeds greater than 14 m/s).

The mechanical power shown in figure 1 was obtained from shaft strain gage measurements and scaled by the 78% efficiency reported in the Annex XIV report. However, in comparing the rotor torque derived power against the generator power, it was found that the efficiency did not match the published efficiency. As a result, a better curve fit between mechanical and generator power was found, as described in equation 1.

$$(1) \qquad P_{Generator} = 0.9036 P_{Mechanical} - 0.847$$

Figure 2 compares the corrected comparison between the generator and mechanical power data. The two sets of data now show better correlation. Also note that they deviate significantly from the NREL power curve at the onset of blade stall (14 - 16m/s wind).
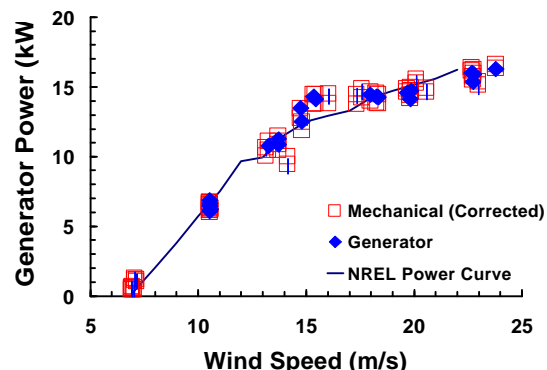


**Figure 2: Corrected power curves**

## Numerical Methods

Three different numerical methods were used to predict the power and aerodynamic loads of the Combined Experiment Phase II rotor. The first method is a BEM method known as YAWDYN/AERODYN developed by Hansen (Refs. 9). The second method is a VL method known as CAMRAD II developed by Johnson (Refs. 10). CAMRAD II was originally developed as a comprehensive vehicle dynamics and aerodynamics code for the rotorcraft industry and has been modified to model horizontal axis wind turbines (HAWT). It utilizes a vortex lattice with free wake (FW) model. In addition, the CAMRAD II code has the capability to run in BEM mode. Both methods have the capability to simulate the dynamic response of the turbines flapping or teetering motions and nacelle yaw.

These methods require two-dimensional airfoil lift and drag data for their predictions. The airfoil of interest for this study is the 21-percent thick S809; an airfoil from the NREL thick-airfoil family for horizontal-axis wind-turbine applications (Ref. 11). For this purpose the airfoil was designed to have a sustained maximum lift, minimal sensitivity of lift to roughness, and low profile drag. An extensive experimental database for use in BEM methods was developed at OSU (Ref. 12).
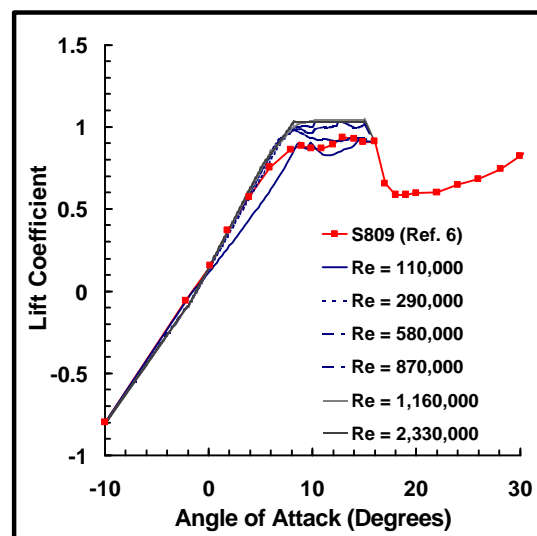


**Figure 3: Lift polar from NREL data and MSES derived**

Airfoil tables were also generated via the MSES code. The MSES multi-element airfoil code (Refs. 13 and 14) represents an extension of the single-element ISES compressible flow airfoil code (Refs. 15 and 16). In this method, the streamline-based Euler equations and boundary-layer equations are solved simultaneously using a full-Newton method. The boundary layers and wakes are described with a two-equation lagged dissipation integral boundary layer formulation and an envelope $e^N$ transition criterion. The initial streamline grid is generated through the solution of a panel method at a specified angle of attack and then modified after each Newton iteration as part of the solution. Displacement bodies based on the shear-layer displacement thickness are used to modify the element surface geometry and are incorporated into the solution after each iteration. This strong inviscid/viscous coupling enables MSES to predict the effects of laminar separation bubbles and other regions of limited flow separation on the pressure distribution.

Two types of airfoil tables were used with CAMRAD II. The first uses the S809 experimental airfoil data obtained from Ref 6. That data consists of $C_l$ and $C_d$ for angles-of-attack from $-2.23^o$ to $89.9^o$ and constructed by NREL from the OSU data. This table was extended to cover a complete angle of attack range of $\pm180^o$.

The second airfoil table uses the MSES code to provide $C_l$ and $C_d$ for several Reynolds numbers. However, since MSES only predicts aerodynamic coefficients up to maximum $C_l$, the S809 experimental data was used beyond stall. Figure 3 illustrates the resulting lift polars used by CAMRAD II.

Inboard of the 30% radius, the airfoil cross section becomes a blend between the S809 and an elliptical cross section as described in Ref. 6. These cross sections result in lift and drag polars that differ greatly from the normal S809 airfoil characteristics. Figure 4 illustrates the difference between the cross section at 16% radius and a normal S809. Attempts to use MSES to construct an airfoil polar for the 16% radius section were not successful. The CAMRAD II calculations presented in this paper used the S809 data at 10% radius. Calculations were also performed assuming that the 16% radius airfoil generated drag but no lift (as a limiting case); the results obtained with this assumption are not presented here since they added little quantitatively and did not change the conclusions at all.



**Figure 4: Inboard airfoil cross sections**

To obtain accurate rotor sectional lift characteristics and hence accurate power prediction, the two-dimensional airfoil data needs to be corrected for inboard stall delay effects. As summarized by Snel and van Holten (Ref. 17), Corrigan and Schillings (Ref. 18), and Du and Selig (Ref. 19) the sectional maximum lift coefficient will exceed the two-dimensional airfoil maximum lift for the inboard sections of a rotor. Corrigan and Schillings developed their stall delay model based upon observations of experimentally measured stall delay on rotors. They applied this model to their helicopter rotor performance code and were able to accurately predict rotor power. Snel and van Holten performed an order of magnitude analysis on the 3-Dimensional boundary layer equations. They show that when the flow begins to separate that the Coriolis force has a significant impact on the spanwise momentum in the boundary layer.

Du and Selig (Ref. 19) developed a stall delay model designed for use in BEM and VL methods. This model is based upon the analysis of 3-D integral boundary layer equations to determine the effects of rotation on boundary layer separation. Equations 2.1-2.6 describe the model as implemented in CAMRAD II.

$$(2.1) \quad c_l = c_{l_{table}} + \left( c_{l_a}(\boldsymbol{a} - \boldsymbol{a}_o) - c_{l_{table}} \right) \bullet w$$

$$(2.2) \quad c_d = c_{d_{table}} + \left( c_{d_o} - c_{d_{table}} \right) \bullet w$$

$$(2.3) \quad w = \frac{1}{2\boldsymbol{p}} \left[ \left( \frac{1.6(c/r)}{.1267} \right) \frac{a - (c/r)^D}{b + (c/r)^D} - 1 \right]$$

$$(2.4) \quad D = \begin{cases} \dfrac{d}{\Lambda r/R} & \text{Lift} \\ \dfrac{d}{2\Lambda r/R} & \text{Drag} \end{cases}$$

$$(2.5) \quad \Lambda = \Omega r / \sqrt{V_{wind}^2 + (\Omega r)^2}$$

$$(2.6) \quad a = b = d = 1.0$$

Where:

$c_l$ and $c_d$ = corrected sectional lift and drag coefficients

$c_{l_a}$ = lift curve slope

$c_{d_o}$ = drag coefficient at zero lift

$c_{ltable}$ and $c_{dtable}$ = 2-D sectional lift and drag coefficients

$\Omega$ = rotor rotational rate

$V_{wind}$ = wind speed

$r$ = local radius

R = tip radius

$c$ = chord

The third numerical method used in this study is a RaNS code known as OVERFLOW developed by Buning, et.al. (Ref. 20). OVERFLOW has been applied to both rotorcraft (Refs. 21,22) as well as a HAWT (Refs. 23). It solves the compressible form of the RaNS equations using an implicit finite difference approach with overset grids.

The grid systems for the phase II rotor consist of 20 overset grid components. All three blades and a simplified hub system are modeled. Each blade was modeled with 5 grids: the tip, the main working part of the blade, the blended parts between the main hub shaft and the main blade, and two grids for the inboard cutout. In addition, the hub grid consists of three overset grids. Figure 5 illustrates the grid systems.

The OVERFLOW code has several options for modeling boundary layer turbulence. One method is an algebraic turbulence model known as Baldwin-Lomax.(Ref. 24). In addition it has a 1-equation model by Baldwin and Barth (Ref. 25). To model transition to turbulence, a laminar region was enforced from the
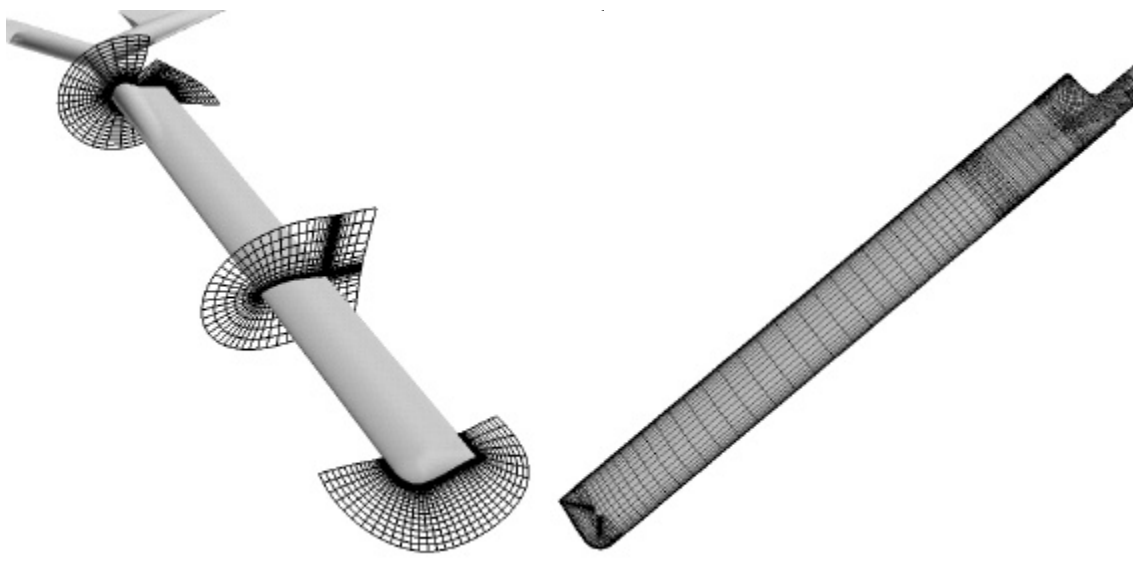
**Figure 5: Overset volume and surface grids of Phase II rotor**

leading edge to ¼ chord location; the turbulence model is then enabled past that point.

## Results

Results for the phase II rotor have been obtained with the three numerical methods and compared against the reduced IEA data. Figure 6 compares the Phase II rotor generator power curves, that was reduced from the IEA Annex XIV data, against the power predictions that were obtained by Aerodyn/Yawdyn, CAMRAD II code (using a free wake, the Du-Selig stall delay model, and the S809 experimental airfoil data), and OVERFLOW. For all the numerical power results, the mechanical power was corrected to generator power using equation 1. All three methods show the ability to model the power at the lower wind speeds. They show
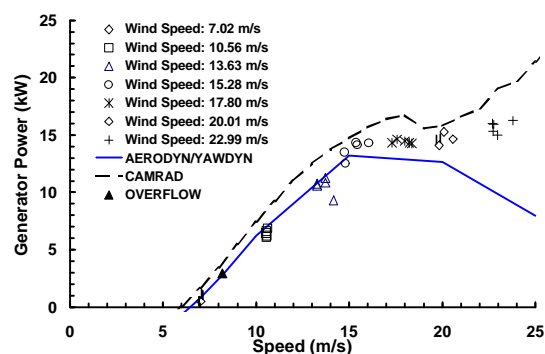
considerable differences however at the higher wind speeds and in predicting maximum power. The stall trends in both the Yawdyn and CAMRAD II results can be directly related to the published airfoil lift and drag tables. The OVERFLOW results agree well at the low wind speed, but grossly overpredicts the power toward the stall region.

Figure 7 illustrates CAMRAD II's ability to predict the power using the different airfoil data with the stall delay model. The S809 result uses the experimental airfoil dataset for the lift and drag as reported in Ref. 6. The MSES results use the airfoil lift and drag polars that take into consideration the Reynolds number variation.

The results show that a free wake based method has the capability to predict the power up to stall. However,
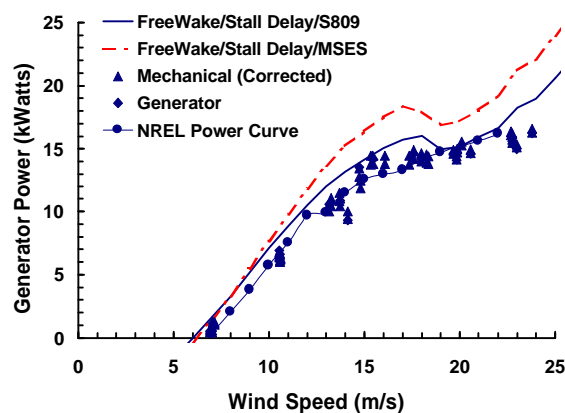


**Figure 6: Comparison of power as predicted by computation methods**



**Figure 7: CAMRAD II power curve Experimental and computed airfoil tables**

the airfoil properties do have a considerable impact on the power prediction. At the lower wind speeds the S809 and MSES results predict approximately the same power. As the rotor approaches stall, the stall delay model amplifies any differences in between the two airfoil tables with the MSES overpredicting the power more than the S809.

Without the stall model, CAMRAD II would underpredict the maximum power. Figure 8 illustrates effect of the stall delay model on the power predicted by the CAMRAD II code using a free wake and experimental S809 airfoil data. The stall delay model has a slight shift in the power for the wind speeds before stall. As expected, it delays the airfoil stall and hence increases the predicted maximum power. However, as implemented, the Du-Selig model places too much stall delay causing an overprediction of the power.
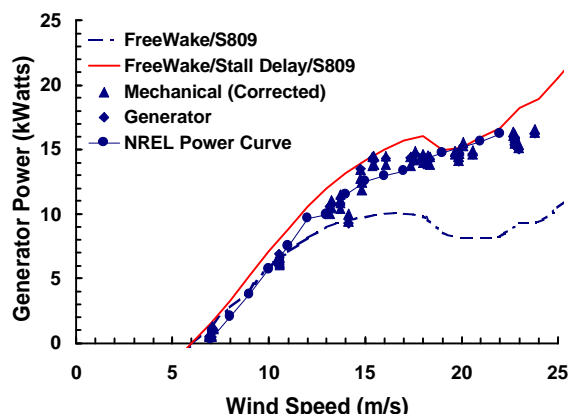


**Figure 8: CAMRAD II Power Curve**
**Free wake, S809 airfoils**
**with and without stall model**

The ultimate goal of the RaNS method is to develop a method capable of predicting the power up through stall. The current method demonstrates the ability to predict the power at wind speeds before stall, but it has difficulty predicting post stall behavior. The following comparisons of the local normal force coefficients illustrate the differences and their causes.

Figure 9 illustrates a comparison of the local normal force coefficient as obtained by the experiment, OVERFLOW, and CAMRAD II. The experimental data shown here was provided by NREL directly to the authors and corresponds to a wind speed of 8.2 m/s. The CAMRAD II data uses either the blade element momentum method or the free wake method. Both utilize the Du-Selig stall delay model with the S809 airfoil table. The

OVERFLOW results shown utilize the Baldwin-Lomax turbulence model with turbulence transition set at the 1/4 chord location. The predictions were computed for the 8.2 m/s condition.
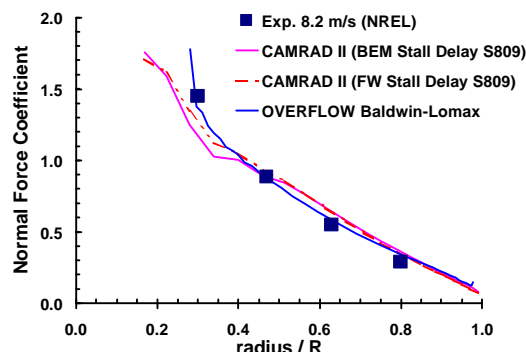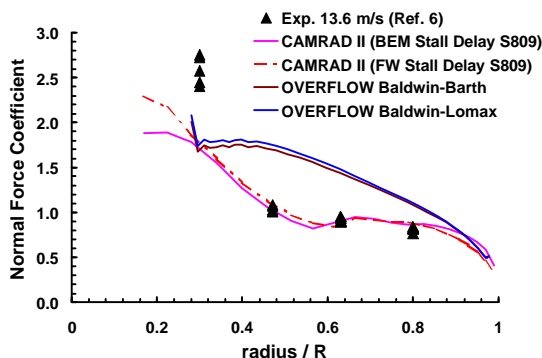


**Figure 9: Cn vs. r/R**
**Comparison between CAMRAD and**
**OVERFLOW, 8.2 m/s average wind speed**

The comparison shows that all three methods do a good job at predicting the spanwise $C_n$ distribution at the pre-stall wind condition of 8.2 m/s. At the outer blade sections, there is little difference between the methods. They have similar trends and little difference in their magnitudes. All along the mid-radial stations, the OVERFLOW code exhibits a better prediction as compared to the 8.2 m/s data. The stall delay method causes this increase in local $C_n$, for the BEM and FW method. On the inboard section, the OVERFLOW code tends to follow the experimental data along with the increased $C_n$ that exceed the 2-D airfoil maximum $C_n$ of 1.0. The CAMRAD II method tends to capture the similar $C_n$ trend.

At the onset of blade stall, the OVERFLOW results begin to deviate from the experiment. Figure 10 illustrates the comparison between the experiment corresponding to the 13.63 m/s average wind speed, the CAMRAD II results, and the OVERFLOW results. Two OVERFLOW derived results are shown. One uses the Baldwin-Lomax turbulence model, while the other uses the Baldwin-Barth turbulence model.

The experimental data shows that for the blade sections outboard from 45% radius, the blade has stalled at a local $C_n$ comparable to the two-dimensional maximum normal force coefficient of approximately 1.0. Stall delay is evident on the inner airfoil sections as shown by the increase in local $C_n$ greater than 1.0. The CAMRAD II result demonstrates an ability to capture the stalled conditions in the outer radial blade locations. They show a rather consistent $C_n$ prediction comparing between the CAMRAD II results and the experimental data. However along the inner radial locations, $r/R \leq 0.4$, the CAMRAD II results begin to deviate in slope and magnitude from the experimental data. At the tip location, there is a slight variation between the BEM and FW
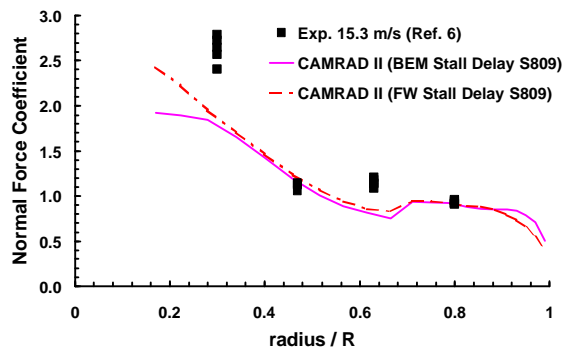
6

**Figure 10: Cn vs. r/R
13.6 m/s average wind speed**



**Figure 12: Cn vs. r/R
15.3 m/s average wind speed**

methods, with the FW method predicting higher tip loading than the BEM method.

The OVERFLOW results show that the RaNS method does not predict the appropriate stall characteristics for the blade. It predicts local $C_n$ comparable to the CAMRAD II code at the outer radial locations of r/R > 0.85. However, it fails to capture the correct stalled behavior over the remainder of the radial locations.

Figure 11 illustrates the pressure distribution and velocity contours as predicted by the RaNS method at r/R = 0.47 and average wind speed of 13.63 m/s. The pressure distribution exhibits a rather high leading edge suction peak characteristic of the S809 at pre-stall conditions. The pressure recovery however, shows little evidence that would indicate boundary layer separation. The flowfield velocity contours further illustrate the failure to stall the local sections. A thick boundary layer forms, but a large separation region fails to form.

Figure 12 illustrates the local normal force coefficient comparison between the CAMRAD II

code and experimental data at the high wind speed of 15.3 m/s. As in the 13.63 m/s wind speed case, the blade has stalled at Cn ~ 1.0 at r/R > 45%. Further inboard, the experiment shows stall delay with an increase in local normal force coefficient up to 2.5 at r/R = 30%. The CAMRAD II code with the stall delay model enabled captures the correct normal force coefficient trends, but misses the correct magnitudes at the inboard and mid radial locations. There is a difference between the BEM and VL methods with the VL method predicting higher tip loading.

## SUMMARY AND CONCLUSIONS

This paper presents the comparisons of Blade Element Momentum, Vortex Lattice and Reynolds Averaged Navier-Stokes wind turbine power predictions. To perform the comparisons, experimental data from the IEA Annex XIV data of the Combined Experiment Phase II rotor was first placed into a form suitable for code validation. Power and blade section normal force coefficient distributions were then used to compare the three methods.
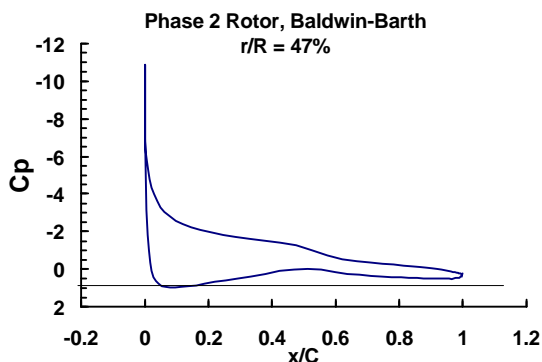


**Figure 11: OVERFLOW pressure distribution and velocity contours
r/R = 47%, 13.6 m/s average wind speed**
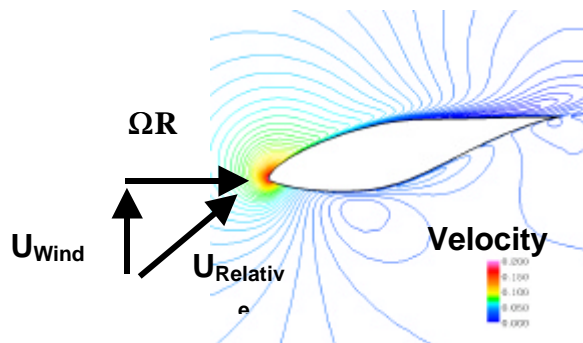
The BEM and VL methods did a fair job at predicting the pre-stall power for the rotor. The vortex lattice with free wake geometry and stall delay proved to be a practical model. A stall delay model is essential for these types of methods. Although the Du-Selig model gives useful results, the current formulation does not work for c/r < 1, it tends to over predict power in the present case. Improved models are needed.

These types of methods also require adequate airfoil tables. The MSES airfoil code gave comparable results to experimental airfoil data but MSES only gave $C_l$-$C_d$ up to $C_{lmax}$. For post stall the method still used experimental $C_l$-$C_d$. This result demonstrated the ability to obtain 2D characteristics from analysis codes. The next step would be to use two-dimensional Navier-Stokes to obtain post stall airfoil data.

The RaNS method was also able to capture the pre-stall aerodynamic behavior, but fails to properly capture the stall behavior. The flow field tends to remain attached at wind speeds that the experimental data indicates should stall the rotor. Further investigation at higher wind speeds is needed. Up coming wind tunnel test of a two-bladed wind turbine will provide valuable steady wind data that may help to improve the RaNS method. In addition, 2-D airfoil static stall studies should be performed using the S809 and the same numerical algorithms as used in the OVERFLOW code.

## ACKNOWLEDGEMENTS

## REFERENCES

[1] Rajagopalan, R.G., Fanucci, J.B., "Finite Difference Model for the Vertical Axis Wind Turbines", Journal of Propulsion and Power, Vol.1, pp.432-436, 1985.

[2] Leclerc, C. and Masson, C, "Predictions of Aerodynamic Performance and Loads of HAWTS Operating in Unsteady Conditions", Proceedings 1999 ASME Wind Energy Symposium, 37th AIAA Aerospace Sciences Meeting and Exhibit, AIAA-99-0066, Reno, NV, January 1999

[3] Whale, J., Fisichella, C.J., and Selig, M.S., "Correcting Inflow Measurements from HAWTS using a Lifting Surface Code", Proceedings 1999 ASME Wind Energy Symposium, 37th AIAA Aerospace Sciences Meeting and Exhibit, AIAA-99-0040, Reno, NV, January 1999

[4] Sorenson, N.N., and Hansen, M.O.L, "Rotor Performance Predictions using a Navier-Stokes Method", Proceedings 1998 ASME Wind Energy Symposium, 36th AIAA Aerospace Sciences Meeting and Exhibit, AIAA-98-0025, Reno, NV, January 1998.

[5] Xu, G., and Sankar, L., "Computational Study of horizontal Axis Wind Turbines", Proceedings 1999 ASME Wind Energy Symposium, 37th AIAA Aerospace Sciences Meeting and Exhibit, AIAA-99-0042, Reno, NV, January 1999

[6] Shepers, J.G., Brand, A.J., Bruining, A., Graham, J.M.R., Hand M.M., Infield, D.G., Madsen, H.A., Paynter, R.J.H., and Simms, D.A., " Final Report of IEA Annex XIV: Field Rotor Aerodynamics", The Netherlands Energy Research Foundation Publication Number ECN-C-97-027, August 1997.

[7] Butterfield, C.P., Musial, W.P., and Simms, D.A., "Combined Experiment Phase I Final Report," NREL TP-257-4655,1992.

[8] Butterfield, C.P., Musial, W.P., and Simms, D.A., "Combined Experiment Final Report - Phase II," NREL TP-422-4807, 1992.

[9] Hansen, A.C. and Laino, D.J., "User's Guide to the Wind Turbine Dynamics Computer Programs YawDyn and AeroDyn for ADAMS" 1999 Available for download from:

http://wind2.nrel.gov/designcodes/yawdyn/

[10] Johnson, W., "Rotorcraft Aerodynamics Models for a Comprehensive Analysis," Presented at the American Helicopter Society Forum, Washington, D.C., May 1998.

[11] Sommers, D.M., "Design and Experimental Results for the S809 Airfoil," NREL/SR-440-6918, January 1997.

[12] Reuss Ramsay, R., Hoffman, M.J., and Gregorek, G.M., "Effects of grit Roughness and Pitch Oscillation on the S809 Airfoil," NREL/TP-442-7817, 1995.

[13] Drela, M., "Newton Solution of Coupled Viscous/Inviscid Multi-Element Airfoil Flows," AIAA Paper 90-1470, June 1990.

[14] Drela, M.,"A User's Guide to MSES 2.95," MIT Computational Aerospace Sciences Laboratory, September 1996.

[15] Giles, M.B. and Drela, M., "Two_Dimensional Transonic Aerodynamic Design Method," AIAA Journal, Vol. 25, No. 9, September 1987, pp. 1199-1206.

[16] Drela, M. and Giles, M.B., "Viscous-Inviscid Analysis of Transonic and Low Reynolds Number Airfoils," AIAA Journal, Vol. 25, No. 10, October 1987, pp. 1347-1355.

[17] Snel, H. and van Holten, Th., "Review of Recent Aerodynamic Research on Wind Turbines with relevance to Rotorcraft, Data and riddles on Dynamic Inflow, Flowfield of Yawed Rotors and Rotating 3-D Stall", Proceeds of the Twentieth European Rotorcraft Forum, October 4-7, 1994.

[18] Corrigan, J.J., and Schillings J.J., "Empirical Model for Stall Delay Due to Rotation", American Helicopter Society Aeromechanics Specialists Conference, San Francisco, CA, January 1994.

[19] Du, Z., and Selig, M., "A 3-D Stall-Delay Model for Horizontal Axis Wind Turbine Performance Prediction", AIAA-98-0021, January 1998.

[20] Buning, P., et.al., OVERFLOW Users Manual ver 1.6ap.

[21] Ahmad, J. and Duque, E.P.N., "Helicopter Rotor Blade Computation in Unsteady Flows Using Moving Overset Grids," Journal of Aircraft, Vol. 33, No. 1, Jan.-Feb. 1996, pp. 54-60.

[22] Meakin, R., "Moving Grid Overset Grid methods for Complete Aircraft Tiltrotor Simulations," AIAA Paper 93-3350, July 1993.

[23] Duque, E.P.N., vanDam, C.P. and Hughes, S., Navier-Stokes Simulations Of The NREL Combined Experiment Phase Ii Rotor, Proceedings 1999 ASME Wind Energy Symposium, 37th AIAA Aerospace Sciences Meeting and Exhibit, AIAA-99-0037, Reno, NV, January 1999

[24] Baldwin, B.S., and Lomax, H., " Thin-Layer Approximation and Algebraic Model for Separated Turbulent Flow, "AIAA Paper 78-0257, Jan 1978.

[25] Baldwin, B.S. and Barth, T.J., "A One-Equation Turbulence Transport Model for High Reynolds Number Wall-Bounded Flows," NASA TM 102847, Aug. 1990.